Imaging Oxysterols in Mouse Brain by On-Tissue Derivatisation – Robotic Liquid Micro-Extraction Surface Analysis – Liquid Chromatography Mass Spectrometry

Eylan Yutuc[1], Roberto Angelini[1], Mark Baumert[2], Natalia Mast[3], Irina Pikuleva[3], Jillian Newton[4], Malcolm R Clench[4], Owain W Howell[1], Yuqin Wang[1], William J Griffiths[1]

[1]Swansea University Medical School, ILS1 Building, Singleton Park, Swansea, SA2 8PP, Wales, UK.

[2]Advion Limited, Harlow Enterprise Hub, Edinburgh Way, Harlow, Essex, CM20 2NQ, UK.

[3]Department of Ophthalmology and Visual Sciences, Case Western Reserve University, Cleveland, OH USA.

[4]Centre for Mass Spectrometry Imaging, Biomolecular Research Centre, Sheffield Hallam University, Howard Street, Sheffield, S1 1WB , U.K.

Abstract

In the current study we describe how we have exploited on-tissue enzyme assisted derivatisation with micro-Liquid-Extraction-for-Surface-Analysis and nano-liquid chromatography-mass spectrometry for the imaging of oxysterols in rodent brain. We find 24S-hydroxycholesterol (24S-HC) to be the most abundant oxysterol in all brain regions being at highest concentration in striatum and thalamus and at lowest levels in grey matter of cerebellum. We are also able, for the first time, to definitively identify 3β,7α-dihydroxycholest-5-en-(25R)26-oic acid in brain, where it is most abundant in cerebellum. We confirm that 24S-HC is essentially absent from brain of the CYP46A1 knockout mouse being replaced by lower levels of 25-hydroxycholesterol.

Introduction

Oxysterols are oxidised forms of cholesterol or of its precursors [Shroepfer 2000]. They are intermediates in steroid hormone and bile acid biosynthesis and possess diverse biological properties [Bjorkhem 2013, Luu 2016]. One of the most well studied oxysterols is 24S-hydroxycholesterol (24S-HC, cholest-5-en-3β,24S-diol). In mammals it is mostly synthesised in neurons by the enzyme cytochrome P450 (CYP) 46A1 and acts as a transport form of cholesterol (Figure 1) [Bjorkhem 2006, Kotti 2009]. Unlike cholesterol, 24S-HC can cross the blood brain barrier (BBB). 24S-HC is a ligand to the liver X receptors (LXRs) [Lehmann 1997], the β-form of which is highly expressed in brain [Wang 2002], and is also a modulator of cholesterol biosynthesis by interacting with the protein INSIG (insulin induced gene) and restricting processing of SREBP-2 (sterol regulatory element-binding protein-2) to its active form as a master transcription factor for cholesterol biosynthesis [Radhakrishnan 2007, Wang 2008]. Despite its potent biological activity, little is known about levels of 24S-HC in distinct brain regions [Heverin 2004, Mast 2017a]. This is also true of the cholestenoic acids, 3β,7α-dihydroxycholest-5-en-(25R)26-oic (3β,7α-diHCA) and 7α-hydroxy-3-oxocholest-4-en-(25R)26-oic (7αH,3O-CA) acids, also formed by enzymatic oxidation of cholesterol, and found in cerebrospinal fluid (CSF), the fluid that bathes the central nervous system (CNS) [Theofilopoulos 2014, Saeed 2014]. 7αH,3O-CA has been suggested to provide an export route for (25R)26-hydroxycholesterol (26-HC, cholest-5-en-3β,(25R)26-diol, also called 27-hydroxycholesterol) which itself passes into the brain from the circulation, but does not accumulate in brain [Meaney 2007]. 3β,7α-diHCA has been shown to be biologically active as a ligand to the LXRs and to be protective towards oculomotor neurons [Theofilopoulos 2014]. Neither acid has previously been definitively identified in brain itself.

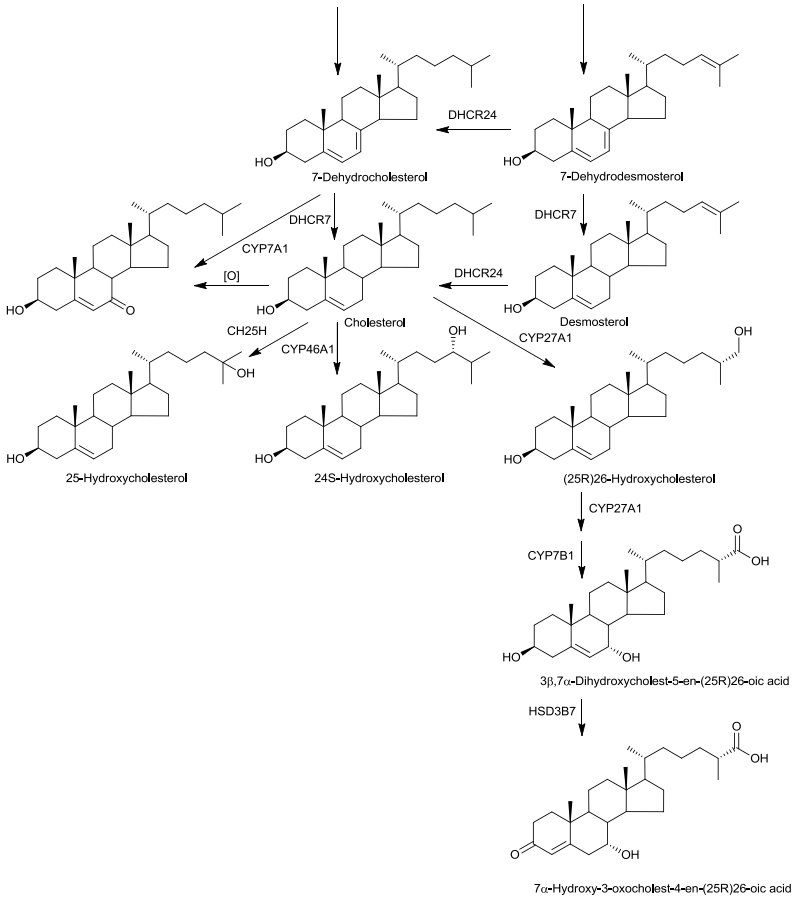

Figure 1. Simplified view of the biosynthesis of oxysterols and sterols investigated in the current study.

The CNS represents a major depository of unesterified cholesterol in mammals, almost 25% of total body cholesterol is found in the CNS where it is present at a level of about 20 μg/mg (wet weight) [Dietschy 2004]. Much of that cholesterol is found in myelin sheaths of oligodendrocytes surrounding the axons of neurons, where it is turned over slowly (0.4%/day in mouse [Dietschy 2004]). A more metabolically active pool is located in intracellular structures such as the endoplasmic reticulum, Golgi apparatus and nucleus of neurons. Here turn-over is estimated at 20% per day [Dietschy 2004]. As cholesterol cannot cross the BBB essentially all cholesterol in brain is biosynthesised in brain. Inborn errors of cholesterol biosynthesis can result in neurodevelopmental disorders and retardation syndromes [Kanugo 2013]. Although cholesterol is the major source of oxysterols, its precursors can also be a source of these molecules [Javitt 2004, Griffiths 2017]. In fact, some cholesterol precursors have biological activity in their own right [Muse 2018]. Desmosterol (cholesta-5,24-dien-3β-ol), the immediate precursor of cholesterol in the Bloch arm of the cholesterol biosynthetic pathway, is both a ligand to the LXRs and also supresses SREBP-2 processing to its active form [Yang 2006, Radhakrishnan 2007]. While levels of cholesterol, desmosterol and other cholesterol precursors have been measured in brain homogenates, fewer studies have been performed to localise these sterols to distinct brain regions [Heverin 2004, Mast 2017a].

To understand better the importance in brain of sterols in general, and oxysterols in particular, it is necessary to correlate molecular concentrations with histology. This can be done by microdissection followed by homogenisation and sterol analysis by mass spectrometry (MS) [Heverin 2004, Mast 2017a]. However, with laboratory animals this is not a simple task. An alternative method to map sterol concentrations in brain is by exploiting mass spectrometry imaging (MSI). This technology pioneered for biological applications by Caprioli and colleagues using matrix-assisted laser desorption ionisation (MALDI) [Norris 2013], has been widely used to image proteins, peptides and lipids in tissues [Berry 2011, Gessel 2014]. MALDI-MSI has been used to image lipids in brain [Trim 2008, Hankin 2011, Zemski Berry 2014], however, cholesterol and other sterols tend to be poorly ionised by conventional MALDI and are underrepresented in MALDI-MSI studies. To enhance ionisation other desorption methods have been employed, including sputtered silver-MALDI [Xu 2015] and silver nanoparticle-MALDI [Roux 2016, Muller 2017]. Silver ions co-ordinate with carbon-carbon double bonds providing cationic adducts of sterols in the MALDI matrix.

MALDI-MSI has been used to image steroid hormones and steroidal drugs in tissue. To achieve this, researchers have utilised on-tissue derivatisation exploiting hydrazine reactions with carbonyl groups (Figure 2) [Cobice 2013, 2016, 2018, Flinders 2015, Barré 2016, Shimma 2016]. Similar reactions have been utilised in "reactive-DESI" (desorption electrospray ionisation), an alternative ionisation technique that can be used for MSI [Badu-Tawiah 2012]. On-tissue derivatisation has also been used in combination with "liquid extraction for surface analysis" (LESA) technology [Cobice 2013, 2016, 2018]. Using LESA, which is based on liquid microjunction surface sampling [Van Berkel 2008], solvent is deposited as a small volume droplet by a robotic sampling probe, i.e. pipette tip or capillary, onto a surface, aspirated back to the tip or capillary and the extract analysed by electrospray ionisation (ESI)-MS. For lipid analysis, the high organic content of the solvent can lead to solvent spreading and low spatial resolution. To minimise this, the sampling probe can be used to make a seal against the tissue surface, thereby preventing solvent spreading and providing higher spatial resolution (400 μm) [Almeida 2015]. The advantage of on-tissue derivatisation in combination with LESA is that low abundance or poorly ionised lipids i.e. steroids and oxysterols, can be targeted through derivatisation, allowing the observation of otherwise undetectable molecules, also giving sufficiently abundant ions for multi-stage fragmentation (MS^n) [Cobice 2013]. Cobice et al using a combination of on-tissue derivatisation MALDI-MSI and LESA-MS^2 have monitored the distribution of corticosteroid in mouse brain tissue and confirmed 7-oxocholesterol (7-OC, 3β-hydroxycholest-5-en-7-one, also called 7-

ketocholesterol) as a substrate for the enzyme 11β-hydroxysteroid dehydrogenase 1 (HSD11B1) and detected testosterone and 5α-dihydrotestosterone in mouse testis [Cobice 2013, 2016].

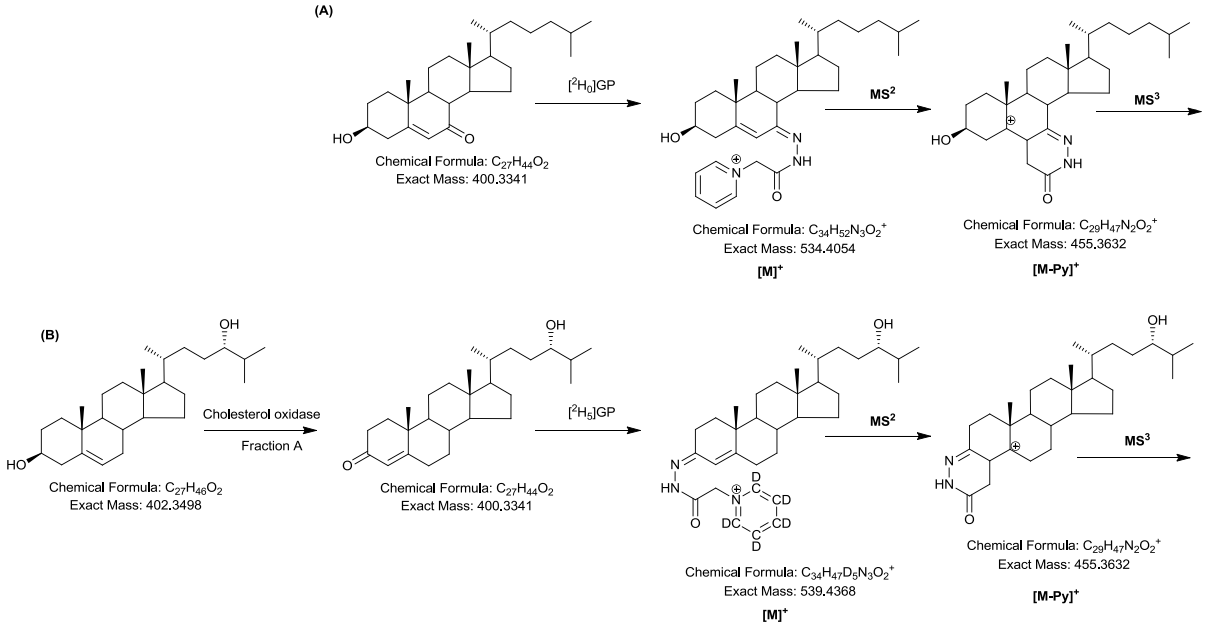

Figure 2. Derivatisation and fragmentation of steroids, sterols and oxysterols exemplified with 7-oxocholesterol, 24S-hydroxycholesterol and with GP hydrazine reagents. (A) Direct derivatisation of oxo compounds. (B) Enzymatic oxidation followed by derivatisation of 3β-hydroxy compounds.

On-tissue derivatisation is problematic for sterols, oxysterols or steroids not possessing a carbonyl group. Hydroxy groups can be targeted for derivatisation but this group common to a wide range of biomolecules and this strategy provides little selectivity. An alternative approach, exploited for in-solution oxysterol analysis, is to utilise bacterial cholesterol oxidase enzyme to specifically convert 3β-hydroxy-5-ene and 3β-hydroxy-5α-hydrogen to 3-oxo-4-ene and 3-oxo-5α-hydrogen structures, respectively, and then derivatise with the Girard hydrazine reagent to provide a charge-tag to the target molecule (Figure 2) [Karu 2007, Roberg-Larsen 2014]. This strategy is termed enzyme-assisted derivatisation for sterol analysis (EADSA). Oxysterols naturally possessing an oxo group, e.g. 7-OC, can be derivatised in parallel in the absence of cholesterol oxidase. A challenge in oxysterol and sterol analysis is that the dominant sterol in mammals is cholesterol, usually being a thousand-fold more abundant than other sterols or oxysterols. Thus, in the absence of chromatography EADSA mass spectra are dominated by cholesterol. In the current study we describe how we have exploited on-tissue EADSA with µLESA and nano-liquid chromatography (nano-LC)-MS(MS^n) for the imaging of oxysterols in rodent brain. We find 24S-HC to be the most abundant oxysterol in all brain regions being at highest concentrations in striatum and thalamus and at lowest levels in grey matter of cerebellum. We are also able for the first time to definitively identify 3β,7α-diHCA in brain, where it is most abundant in cerebellum. We confirm that 24S-HC is essentially absent from brain of the CYP46A1 knockout mouse (CYP46A1-/-) being replaced by lower levels of 25-hydroxycholesterol (25-HC, cholest-5-en-3β,25-diol).

Experimental

Chemicals and Reagents

HPLC grade methanol and water were from Fisher Scientific (Loughborough, UK). Glacial acetic and formic acids were purchased from VWR (Lutterworth, UK). [25,26,26,26,27,27,27-$^2H_7$]22S-hydroxycholesterol ([$^2H_7$]22S-HC, [25,26,26,26,27,27,27-$^2H_7$]cholest-5-ene-3β,22S-diol) and

[25,26,26,26,27,27,27-$^2H_7$]24R/S-hydroxycholesterol ([$^2H_7$]24R/S-HC) were from Avanti Polar Lipids (Alabaster, AL). [25,26,26,26,27,27,27-$^2H_7$]22S-hydroxycholest-4-en-3-one ([$^2H_7$]22S-HCO) was prepared from [$^2H_7$]22S-HC as described in Crick et al [Crick 2015]. Cholesterol oxidase from *Streptomyces sp.* and potassium dihydrogen phosphate were from Sigma-Aldrich (Dorset, UK). [$^2H_0$]Girard P ([$^2H_0$]GP) from TCI Europe (Zwijndrecht, Belgium). [$^2H_5$]GP was synthesised as described by Crick et al [Crick 2014, Crick 2015].

Tissue sectioning

Mouse brain was from male 4-month-old *Cyp46a1-/-* and wild type (WT *Cyp46a1+/+*, C57BL/6J;129S6/SvEv) littermates as detailed in [Mast 2017b]. Fresh frozen tissue, mounted in OCT, was cryo-sectioned using a Leica Cryostat CM1900 (Leica Microsystems, Milton Keynes, UK) at a chamber temperature of -16°C into 10 µm-thick sections which were thaw-mounted onto glass microscope slides and stored at -80°C until use. Luxol Fast Blue and Cresyl Violet staining was performed on tissue sections adjacent to sections analysed by MSI.

Deposition of internal standard and on-tissue EADSA.

Frozen tissue sections were dried in a vacuum desiccator for 15 min after which the internal standards [$^2H_7$]22S-HC, [$^2H_7$]22S-HCO and [$^2H_7$]24R/S-HC (5 ng/µL of each in ethanol) were sprayed from a SunCollect automated pneumatic sprayer (KR Analytical Ltd, Cheshire, UK) at a flow rate of 20 µL/min at a linear velocity of 900 mm/min with 2 mm line distance and Z position of 30 mm in a series of 18 layers. The resulting density of each deuterated standard was 1.87 ng/mm^2. The sprayer was thoroughly flushed with about 2 mL of methanol after which cholesterol oxidase (0.264 units/mL in 50 mM KH_2PO_4 pH7) was sprayed for 18 layers. The first layer was applied at 10 µL/min, the second at 15 µL/min, then all the subsequent layers at 20 µL/min to give an enzyme density of 0.1 munits/mm^2. Thereafter, the enzyme-coated slide was placed on a flat dry bed in a sealed pipette tip box (11.9 cm x 8.2 cm x 8.5 cm) above 30 mL of warm water (37 ^{o}C), then incubated at 37°C for 1 hr. Afterwards, the slide was removed and dried in a vacuum desiccator for 15 mins. [$^2H_5$]GP (6.3 mg/mL in 70% methanol with 5% acetic acid) was sprayed on the dried slide with the same spray parameters as used for spraying cholesterol oxidase. The resulting GP density was 2.35 mg/mm^2. The slide was then placed on a flat dry table in a covered glass chamber (12 cm x 12 cm x 7.2 cm) containing 30 mL of pre-warmed (37 ^{o}C) 50% methanol, 5% acetic acid and incubated in a water bath at 37°C for 1 hr. The slide was removed and dried in a vacuum desiccator until MSI analysis. To analyse sterols containing a naturally occurring oxo group, [$^2H_7$]22S-HCO was used as the internal standard, the cholesterol oxidase spray step was omitted and [$^2H_0$]GP (5 mg/mL in 70% methanol with 5% acetic acid) used as the derivatisation agent.

Robotic Liquid Micro-Extraction Surface Analysis (µLESA)

Oxysterols on the surface of brain tissue were sampled using a TriVersa Nanomate (Advion, Ithaca, NY) with a modified capillary extraction probe (LESAplus). The Advion ChipsoftX software was used to capture an optical image of the prepared slide on a flatbed scanner prior to analysis. The same software was also used to define extraction points on the tissue. A 330 µm i.d. / 790 µm o.d. FEP (fluorinated ethylene propylene, a copolymer of hexafluoropropylene and tetrafluoroethylene) sleeve was attached to a 200 µm i.d. / 360 µm o.d. fused silica capillary held in a mandrel of the Advion TriVersa Nanomate, this created a seal when in contact with tissue preventing the dispersion of extraction solvent (50% methanol) and limiting the sampling area to the internal diameter of the FEP sleeve (Figure 3). Three µL of extraction solvent was aspirated into the capillary from the solvent reservoir, the mandrel moved robotically to an exact tissue location and 1 µL of solvent dispensed on-

tissue and held for 30 s before being aspirated back into the capillary. The mandrel moved once again, and the extract was dispensed into a well of a 384-well plate. The process was repeated twice more with extract dispensed into the same well, before the combined extract was injected via the extraction probe into the sample loop of the nano-LC system (see below). The entire procedure was then repeated on a new extraction point. Multiple points were analysed to build up an oxysterol image of brain tissue.

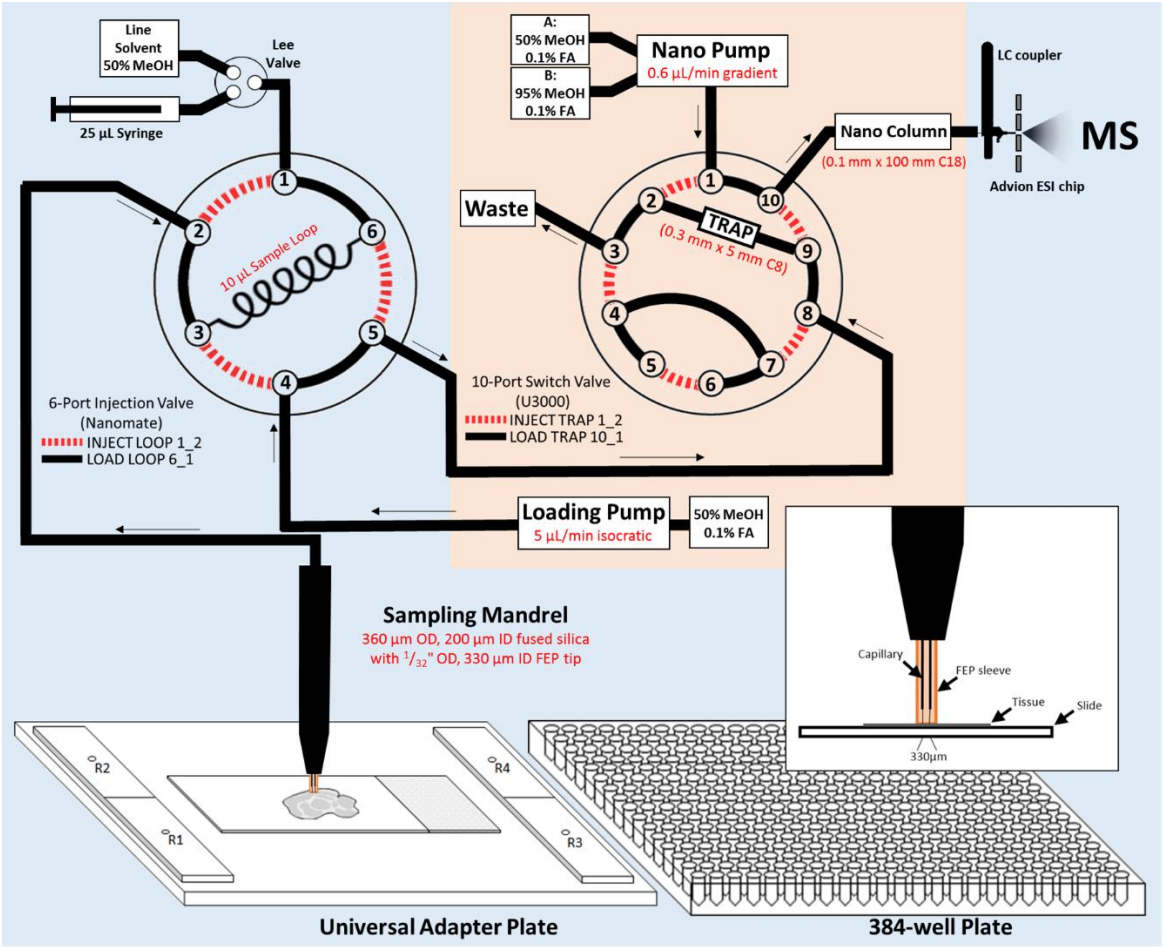

Figure 3. Schematic representation of the of the µLESA system linked to the nano-LC. With connections between ports 1 and 6 and between 2 and 3 the 6-port injection valve is in the load position. Once loaded connections are made between ports 4 and 3 and between 6 and 5. Sample is transported to the 10-port valve and with connections made between ports 8 and 9 and 2 and 3, sterols are trapped on the C_8 trap-column. Port 1 is then collected to 2, 9 to 10 and sterols eluted from the trap column to the analytical nano-column.

Nano-LC-MS(MS^n)

Nano-LC separations were performed on an Ultimate 3000 UHPLC system (Dionex, now Thermo Scientific, Hemel Hempstead, UK). The µLESA extract was delivered from the sample loop onto a trap column (HotSep Tracy C_8, 5 µm 100 Å, 5 mm x 0.3 mm, Kinesis Ltd, Bedfordshire, UK) using a loading solvent of 50% methanol, 0.1% formic acid at a flow-rate of 5 µL/min. The trap column eluent containing unretained GP reagent was delivered to waste (Figure 3). After 13 min the trap column was switched in-line with the analytical column (ACE C_{18}, 3 µm 100 Å, 100 mm x 0.1 mm, Aberdeen,

Scotland) and a gradient delivered by the binary nanopump at 0.6 µL/min. Mobile phase A consisted of 50% methanol, 0.1% formic acid and mobile phase B consisted of 95% methanol, 0.1% formic acid. After 8 min at 20% B, the proportion of B was raised to 60% B over the next 10 min and maintained at 60% B for 5 min, then raised again to 95% B over 5 min and maintained at 95% B for a further 38 min before returning to 20% B in 1 min and re-equilibrating for 11 min, giving a total run time of 78 min. The trap-column was switched out of line and re-equilibrated for 11 min prior to the next injection. The eluent was directly infused into an Orbitrap Elite mass spectrometer (Thermo Scientific, Hemel Hempstead, UK) using the Nanomate chip-based nano-ESI (Advion, Ithaca, NY) set at between 1.7 and 2.0 kV chip voltage. To avoid cross-contamination between samples a column wash with injection of 10 µL 100% propan-2-ol and a fast gradient of 36 min was performed between injection of tissue extracts. The 100% propan-2-ol "plug" was delivered to the trap column and washed for 5 min before switching in-line with the analytical column for further washing. For column washing the proportion of B was raised from 20% to 95% within 5 min and maintained at 95% B for 19 minutes after which it returned to 20% within 1 minute. The trap was then switched off-line and the analytical column equilibrated for a further 11 minutes before the next sample was injected.

For each injection five scan events were performed: one high resolution scan (240,000 full-width at half maximum height definition at *m/z* 400) in the Orbitrap analyser in parallel to four MS^3 scan events in the linear ion-trap. Quantification was by isotope dilution using tissue-coated isotope-labelled standard. MS^3 for were the transitions $[M]^+ \rightarrow [M\text{-}Py]^+ \rightarrow$, where Py is the pyridine group of the GP-derivative (Figure 2).

Quantification

To achieve reliable quantitative measurements an isotope labelled internal standard $[^2H_7]$24R/S-HC (for use with cholesterol oxidase) or $[^2H_7]$22S-HCO (for use in the absence of cholesterol oxidase) was sprayed on-tissue prior to the EADSA process (see above). This process corrects for variation in surface extraction, injection volume, and MS response.

Results

Analytical Platform

The platform was designed to allow the MSI of oxysterols in tissue against a large background of cholesterol and other more readily ionised lipids. To meet this challenge, we have used on-tissue derivatisation in combination with µLESA and nano-LC-$MS(MS^n)$. Each of the system components required optimisation.

On-tissue EADSA

The protocol for on-tissue enzymatic oxidation of sterols (Figure 2) was adapted from the procedure used in solution using cholesterol oxidase enzyme in KH_2PO_4 buffer [Karu 2007], the only difference being enzyme was sprayed onto tissue in buffer and then incubated at 37 °C in a humid chamber rather than being in solution. In trial experiments after a 1 hr incubation period at 37 °C there was no evidence for any non-oxidised sterol. The next step in the method was on-tissue derivatisation of oxo-containing sterols (Figure 2). Others have used Girard T hydrazine as the derivatising agent [Cobice 2013, 2016, 2018, Flinders 2015, Barré 2016, Shimma 2016], however, based on our experience of using the GP reagent for in-solution derivatisation of oxysterols, GP hydrazine was used here [Karu 2007]. The disadvantage of using GT hydrazine is that the major MS^2 fragmentat-ion is $[M\text{-}59]^+$ and the exact same neutral-loss is observed in the fragmentation of endogenous glycerophosphocholine lipids. With $[^2H_0]$GP the major MS^2 fragment-ion is $[M\text{-}79]^+$ and for $[^2H_5]$GP $[M\text{-}84]^+$, neutal-losses not

common for other lipids. We sprayed a similar concentration of GP reagent (6.3 mg/mL for [$^2H_5$]GP or 5 mg/mL [$^2H_0$]GP) in the same solvent as previously used for in-solution derivatisation (70% methanol 5% acetic acid) [Karu 2007]. As in reported studies using GT reagent [Cobice 2013, 2016, Barre 2016] it was essential to incubate the GP-coated tissue in a humid atmosphere to achieve derivatisation. Initial tests in a dry atmosphere revealed no derivatisation of 3-oxo-4-ene substrates. Incubation in a humid chamber (12 cm x 12 cm x 7.2 cm) containing 30 mL of 50% methanol, 5% acetic acid at 37°C for 1 hr provided an efficient derivatisation environment with minimum lateral dispersion of analytes. Increasing the volume or organic content of solution lead to lipid delocalisation, while reducing the volume and organic content provided less efficient derivatisation based on ion-current in µLESA-MS measurements. For comparison, Cobice et al sprayed GT hydrazine at 5 mg/mL in 80% methanol 0.1% trifluoroacetic acid and incubated in a sealed Petri dish containing 2 mL of water or in a sealed slide box at 80% humidity, for 60 min at 40 ^oC [Cobice et al 2013, 2016].

µLESA

Using conventional LESA, a pipette tip is positioned above the target surface and dispenses a µL-volume of extraction solvent to create a liquid microjunction with the surface. Solvent is then aspirated back to the tip after a sufficient time has elapsed for surface-liquid analyte extraction. The pipette tip containing extract is then robotically transferred to a nano-ESI chip for MS analysis [Almedia 2015]. Spatial resolution using this format is typically >1 mm in diameter [Almeida 2015]. The LESAplus configuration of the TriVersa Nanomate incorporates a 200 µm i.d. / 360 µm o.d. fused silica capillary replacing the pipette tip, this when used with water-rich extraction solvents can improve spatial resolution to less than $\leq$1 mm [Lamont 2017, Ryan 2018]. However, when using a 50% methanol solvent we were unable to achieve this degree of spatial resolution as the surface tension required for a stable liquid microjunction was not attainable. To overcome this problem a 330 µm i.d. / 790 µm o.d. FEP sleeve was attached to the fused silica capillary and used to make a direct seal with the tissue surface preventing spreading of the extraction solvent beyond the boundary of the sleeve (Figure 4). This gave spatial resolution of <400 µm as assessed by microscopic evaluation of tissue after liquid extraction (Figure 4). A 50% methanol extraction solvent was selected as this was the same methanol content to that used in the loading for nano-LC (see below). The volume of solvent dispensed onto tissue and the extraction time were optimised to maximise oxysterol extraction without compromising spatial resolution. This was assessed by MS ion-current for target oxysterols. The number of repeat extractions on the same spot was similarly optimised. The optimal conditions were a dispensed volume of 1 µL, an extraction time of 30 s, performed three times on the same spot.

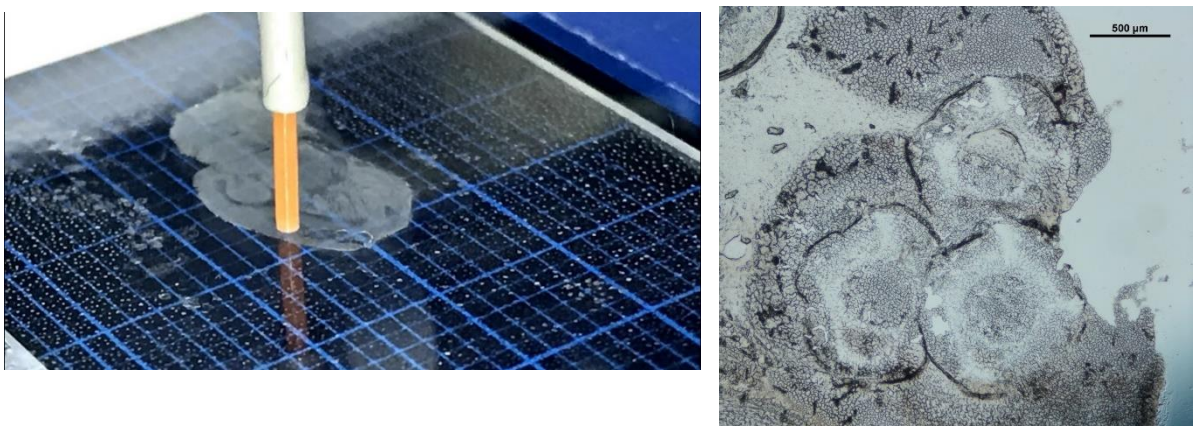

Figure 4. Modification of the LESAplus configuration to provide a direct seal with tissue surface preventing spreading of organic solvent. Left panel, FEP sleeve (orange) surrounding a fused silica

capillary making a direct seal on a section of mouse brain tissue. Right panel, microscope view of imprints made after LESA sampling of brain tissue. The inner circles define the extraction area, the outer circles define the outer diameter of the FEP sleeve.

Nano-LC

The nano-LC system was based on the conventional reversed-phase LC system routinely used for oxysterol analysis after EADSA [Karu 2007] modified by Roberg-Larsen et al for nano-LC [Roberg-Larsen 2014]. By incorporating of a reversed-phase trap column prior to the analytical column it was possible to trap GP-derivatised sterols and wash to waste unreacted GP reagent and polar analytes (Figure 3). After a washing period of 13 min, the trap column was back-flushed to the C_{18} analytical column. The gradient was optimised for analysis of oxysterol in brain allowing separation of the major oxysterol, 24S-HC, from the major sterol, cholesterol, and its precursors desmosterol and 7-dehydrocholesterol (7-DHC, cholesta-5,7-dien-3β-ol). To avoid cross-contamination between samples a column wash with an injection of 10 µL 100% propan-2-ol and a fast gradient of 36 min was performed between injection of samples. Carry-over into this wash for 24S-HC and cholesterol was <2%. This procedure eliminated carry-over of oxysterols into the next sample. Relative standard deviation of retention-time for 24S-HC was 0.3% ± 0.1% (mean ± SD) over five successive injections of derivatised brain tissue.

Oxysterols in Mouse Brain

Previous studies using MS have defined concentration of 24S-HC, the major oxysterol in mouse brain, to be of the order of 20 – 60 ng/mg [Ogundare 2010, Meljon 2014, Mast 2017b]. After EADSA treatment, µLESA-nano-LC-MS analysis of 400 µm i.d. spots of brain tissue gave intense peaks for 24S-HC in reconstructed ion chromatograms (RICs) for $[M]^+$ at *m/z* 539.4368 ± 10 ppm (Figure 5A, upper panel) and in total ion chromatograms (TICs) for the multiple reaction monitoring (MRM) transition 539.4→455.4→ (Figure 5B). In the absence of chromatography only cholesterol is observed (Figure 5E). Relative quantification between spots was achieved using $[^2H_7]$24R/S-HC sprayed on tissue to density of 1.87 ng/mm^2. Peak area ratios determined from RICs at *m/z* 539.4368 ± 10 ppm (24S-HC) and 546.4807 ± 10 ppm ($[^2H_7]$24R/S-HC) gave a value of about two for 24S-HC/$[^2H_7]$24R/S-HC in brain cortex and about three in striatum (Figure 5A). Analysis of six adjacent spots in the cortical region gave a mean ratio of 1.08 with a relative standard deviation of 6 %. This corresponds to a density of 24S-HC of 2.01 ± 0.12 ng/mm^2 (mean ± SD).

(A)

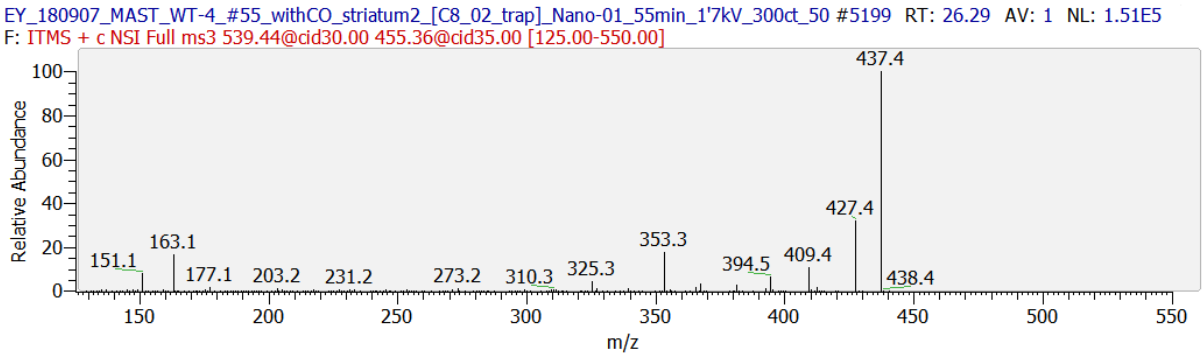

(B)

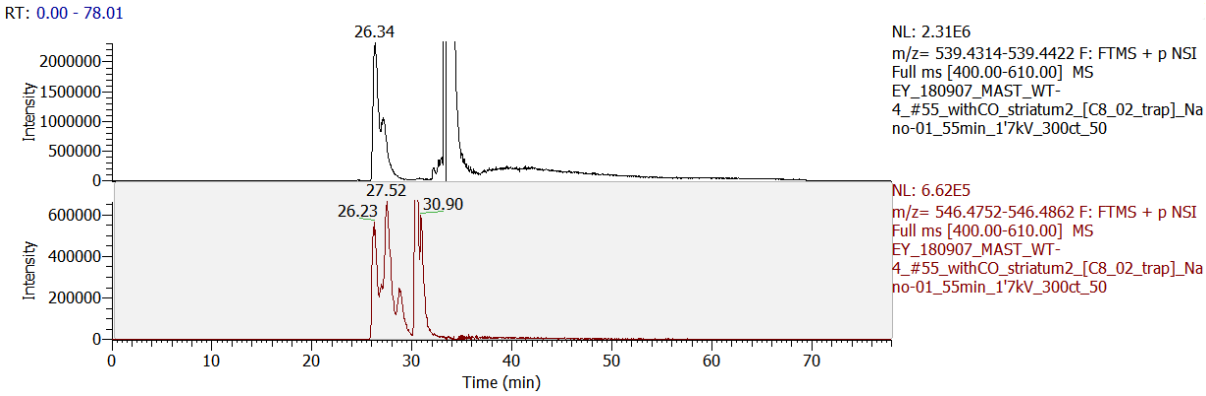

(C)

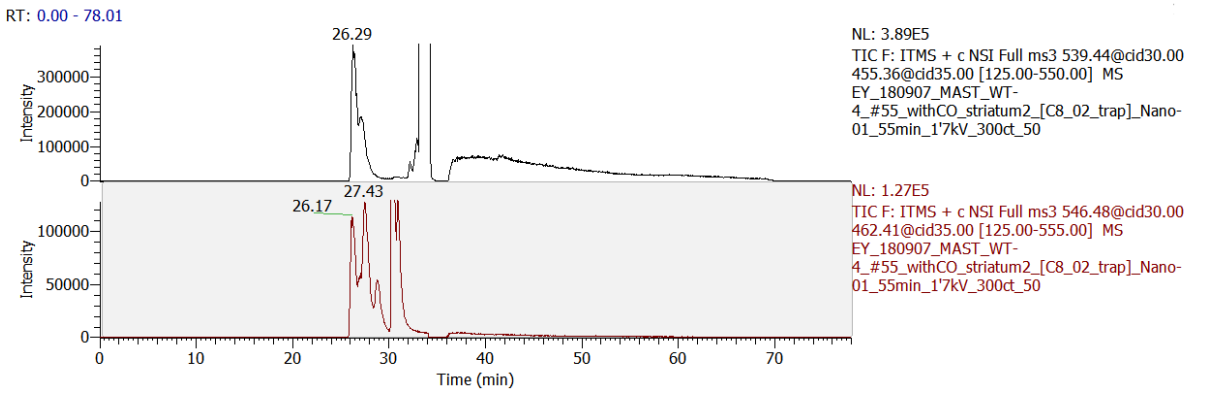

(D)

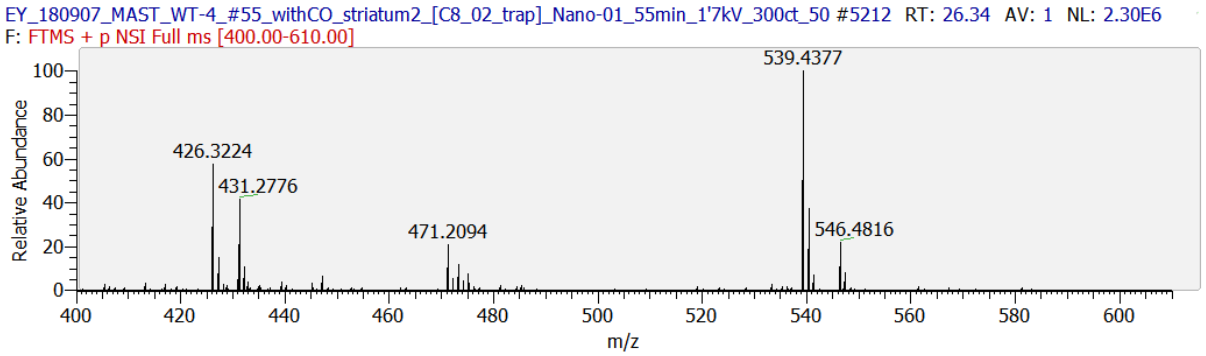

(E)

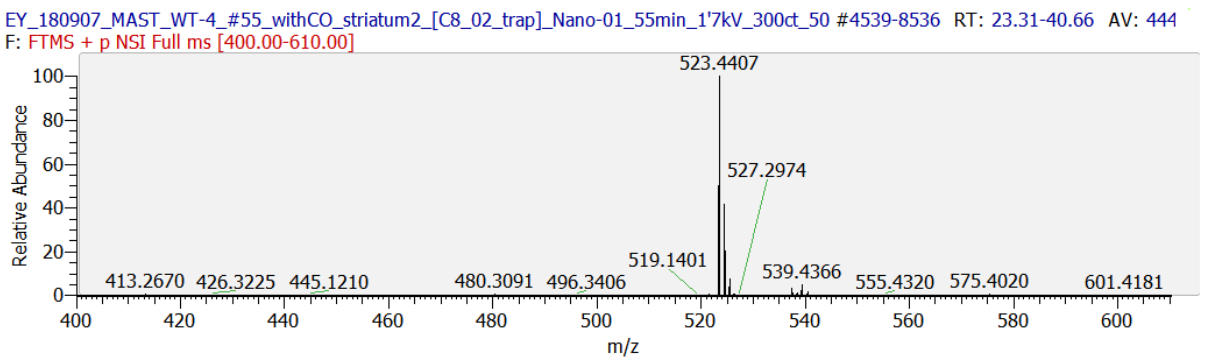

Figure 5. µLESA-nano-LC-MS following EADSA treatment of mouse brain. (A) RIC for the $[M]^+$ ion of 24S-HC (*m/z* 539.4368 ± 10 ppm) and $[^2H_7]$24R/S-HC (546.4807 ± 10 ppm). (B) TIC for the MRM transitions $[M]^+ \rightarrow [M\text{-}Py]^+ \rightarrow$ for 24S-HC and $[^2H_7]$24R/S-HC. (C) Mass spectrum recorded at 26.34 min. (D) MS^3 spectrum recorded at 26.29 min. (E) Summed mass spectrum over the entire chromatogram. Note that 24S-HC appears as a major chromatographic peak with a shoulder, this is a consequence of unresolved *syn* and *anti* conformers of the GP-derivative. Similarly, each of the R and S epimers of the $[^2H_7]$24R/S-HC mixture give *syn* and *anti* conformers which are only partially resolved.

Nine brain regions, isocortex, striatum, thalamus, hippocampus, midbrain, pons, medulla, cerebellum (grey matter) and cerebellum (white matter) were analysed by µLESA-nano-LC-MS (Figure 6). As is evident from Figure 7, 24S-HC is least abundant in the grey matter of the cerebellum and most abundant in the striatum and thalamus. Similar data was obtained from sagittal sections from three different mice. In all mice 24S-HC was found to be most abundant in striatum and thalamus and least abundant in cerebellum.

(A)

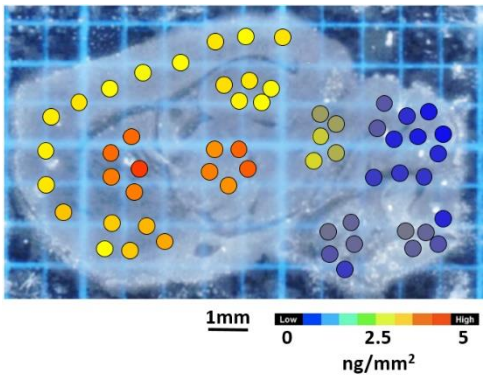

(B)

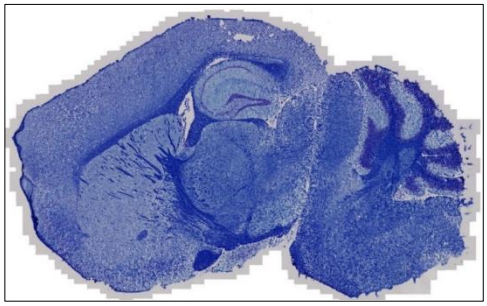

(C)

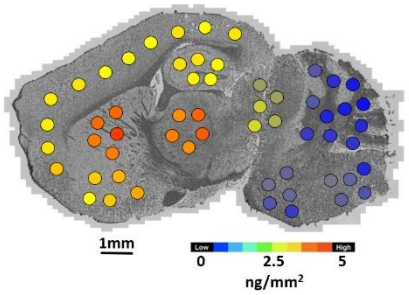

Figure 6. Sagittal section of mouse brain analysed by µLESA-nano-LC-MS. (A) Photograph of mouse brain slice showing spots analysed by µLESA-nano-LC-MS. Concentration of 24S-HC in the spots analysed is indicated by colour on a blue to red scale (B) Luxol Fast Blue and Cresyl Violet stained brain slice adjacent to slice analysed by µLESA-nano-LC-MS.(C) Concentration of 24S-HC superimposed on the stained slice.

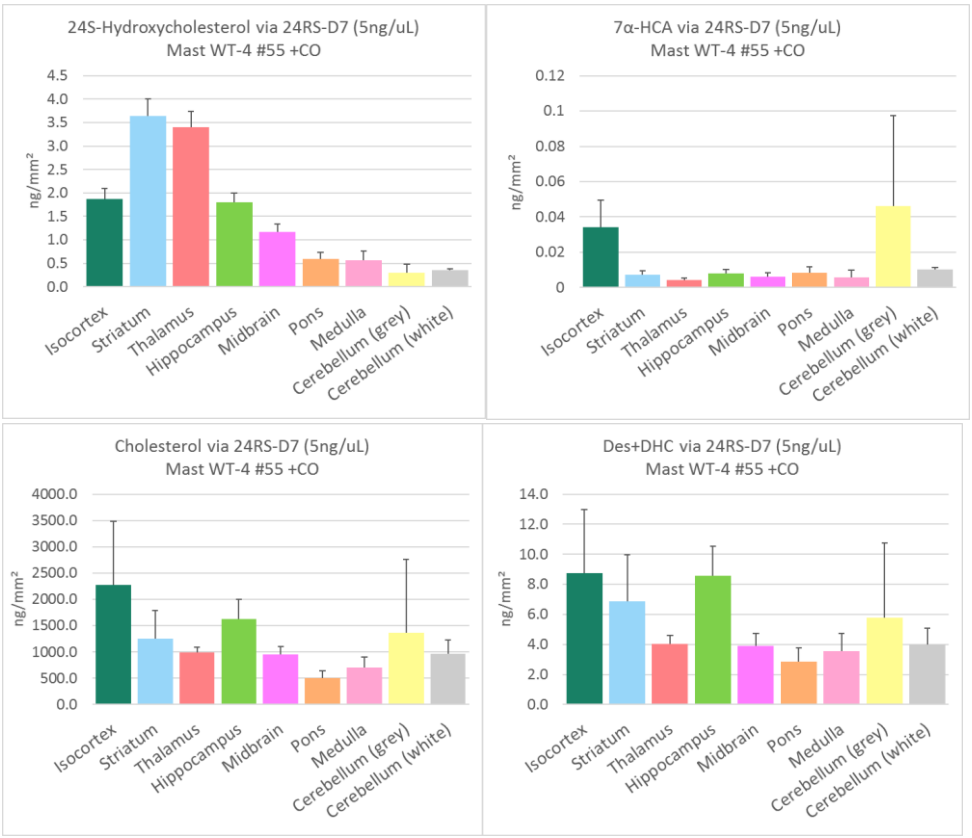

Figure 7. Concentrations of sterols in mouse brain determined by µLESA-nano-LC-MS. Top left 24S-HC. Top right 3β,7α-diHCA + 7αH,3O-CA. Bottom left cholesterol. Bottom right 7-DHC + desmosterol.

Previous studies have suggested that 26-HC is converted by CYP7B1 and CYP27A1 in brain to 3β,7α-diHCA and 7αH,3O-CA (Figure 1) [Meaney 2007, Theofilopoulos 2014, Iuliano 2015], we thus generated RIC and TIC for the appropriate *m/z* 569.4110 ± 10 ppm and MS^3 transition $[M]^+ \rightarrow [M\text{-}Py]^+ \rightarrow$, i.e. 569.4→485.3→ (Figure 8A&B). When using EADSA with cholesterol oxidase the combination of 3β,7α-diHCA plus 7αH,3O-CA is measured. The levels of the individual analytes are deconvoluted by repeat analysis on an adjacent section of brain tissue in the absence of cholesterol oxidase enzyme using $[^2H_7]$22S-HCO internal standard and $[^2H_0]$GP reagent. Here 7αH,3O-CA is measured but not 3β,7α-diHCA. The combination of 3β,7α-diHCA plus 7αH,3O-CA was evident at concentrations near the limit of detection (Figure 7). In the absence of cholesterol oxidase treatment 7αH,3O-CA was detected, but at concentrations close to the limit of detection (Figure 8E&F).

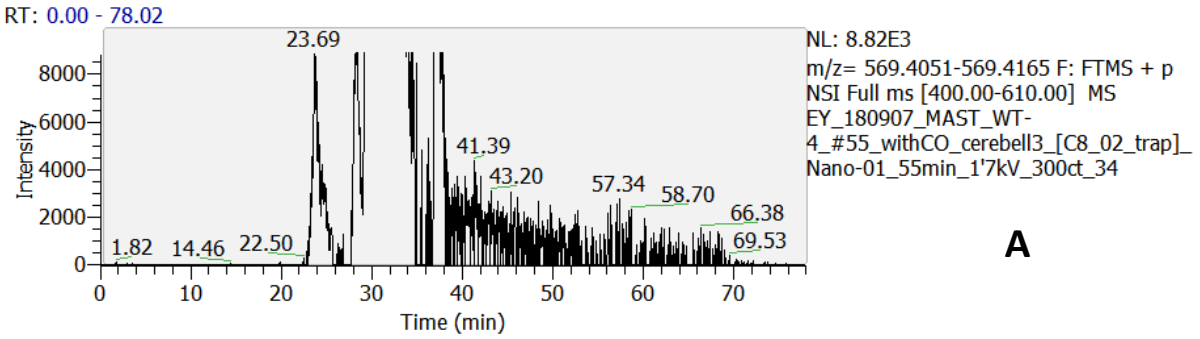

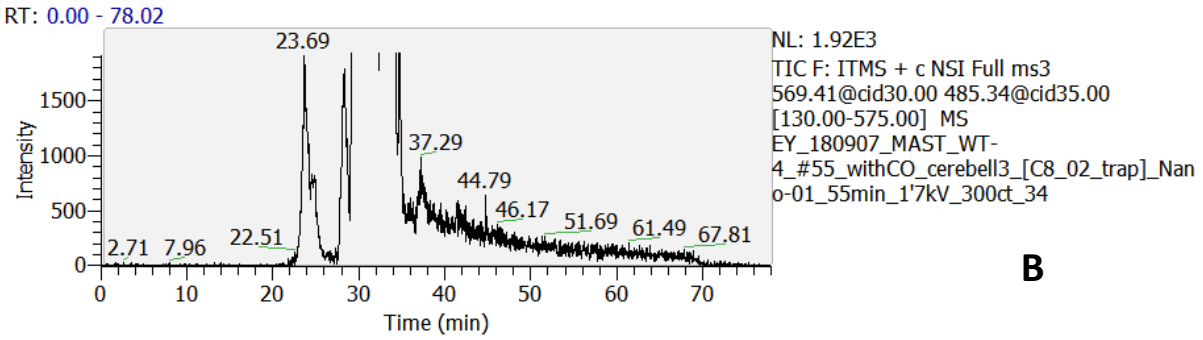

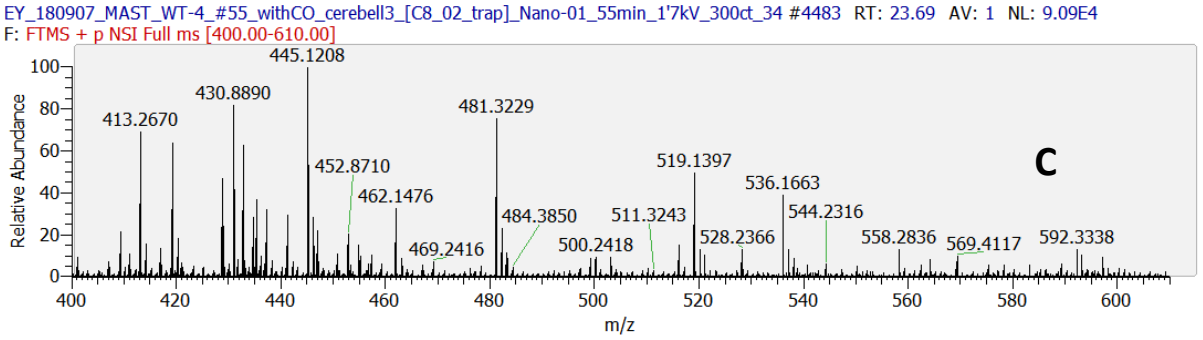

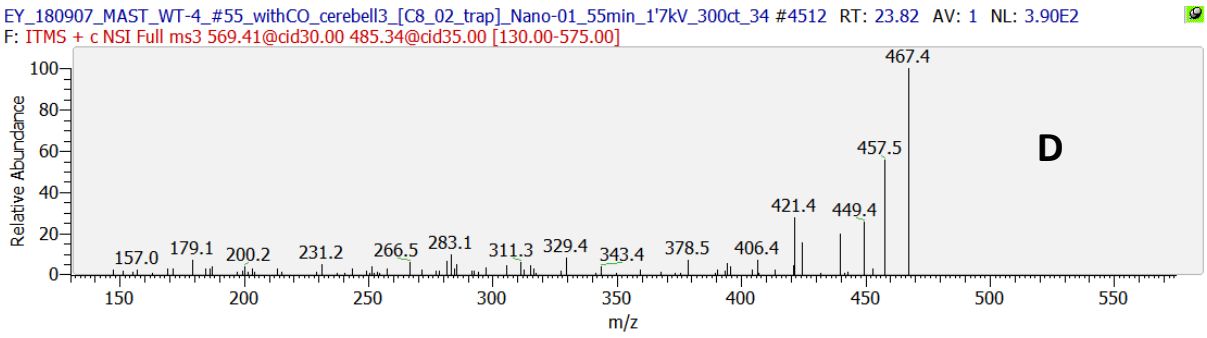

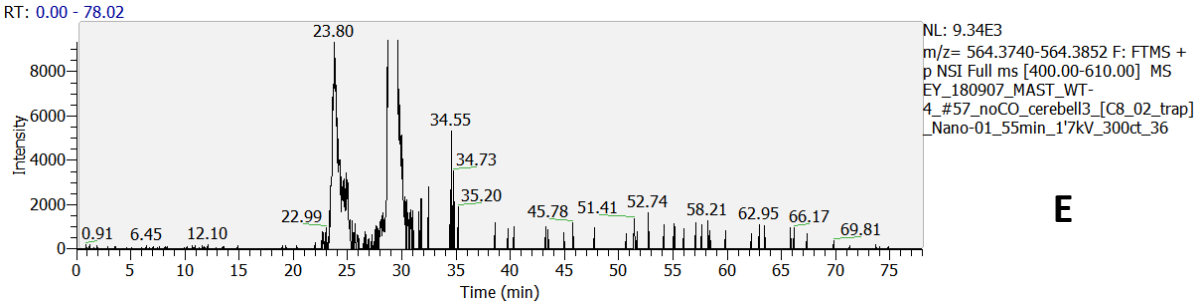

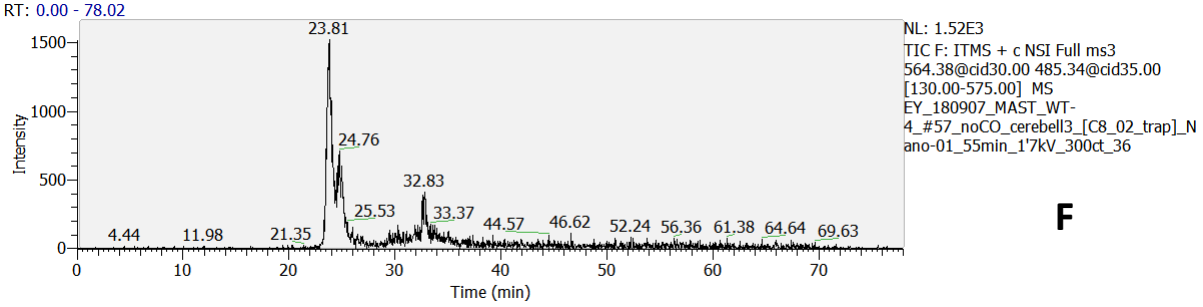

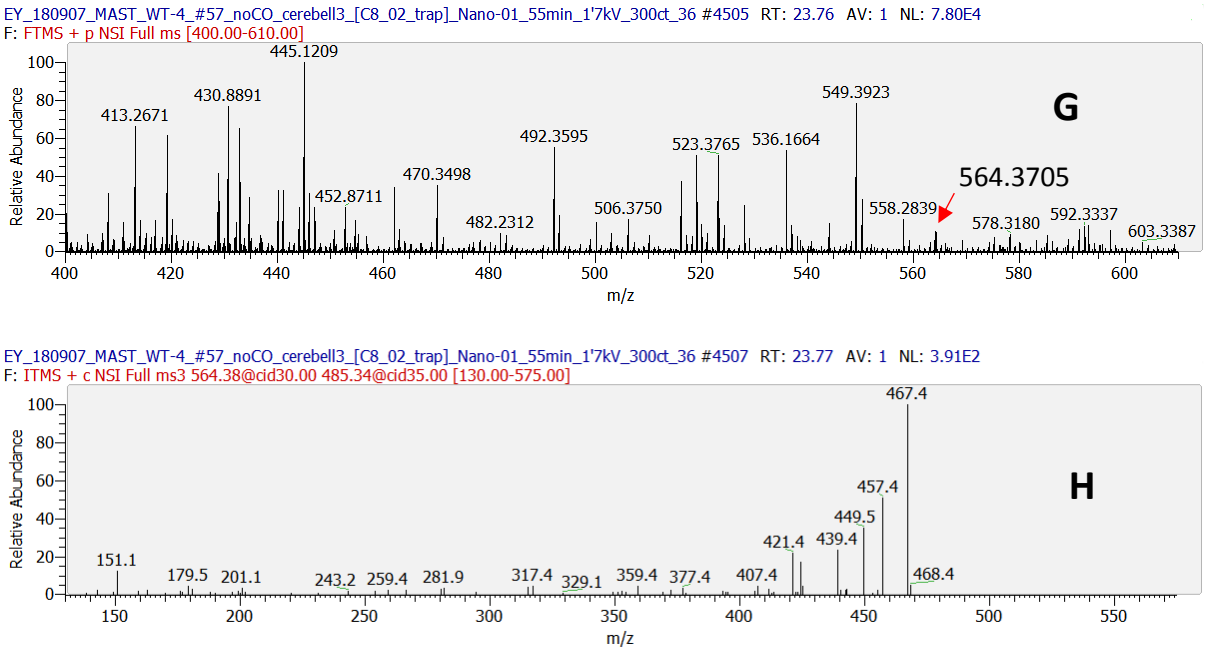

Figure 8. µLESA-nano-LC-MS of mouse brain following treatment with (A-D) or without (E-H) cholesterol oxidase. (A) RIC for the $[M]^+$ ion of 3β,7α-diHCA plus 7αH,3O-CA (*m/z* 569.4110 ± 10 ppm). (B) TIC for the transitions $[M]^+ \rightarrow [M\text{-}Py]^+ \rightarrow$ for 3β,7α-diHCA plus 7αH,3O-CA. (C) Mass spectrum recorded at 23.69 min. (D) MS^3 spectrum recorded at 23.82 min. (E) RIC for the $[M]^+$ ion of 7αH,3O-CA (*m/z* 564.3796 ± 10 ppm). (F) TIC for the transitions $[M]^+ \rightarrow [M\text{-}Py]^+ \rightarrow$ for 7αH,3O-CA. (G) Mass spectrum recorded at 23.76 min. (H) MS^3 spectrum recorded at 23.77 min.

7-OC has previously been detected in brain using Girard derivatisation and LESA-MS [Cobice 2013]. The presence of a natural 7-oxo-5-ene structure allows Girard derivatisation in the absence of cholesterol oxidase enzyme. To investigate the presence of 7-OC and its isomer 7α-hydroxycholest-4-en-3-one (7α-HCO) the brain slice prepared in the absence of cholesterol oxidase were used. Only low levels of 7-OC and 7α-HCO were present.

Cholesterol and its precursors in mouse brain

In the current study focus was on oxysterol rather than on cholesterol and its precursors. Never-theless it was possible to make approximate measurements for cholesterol and the sum of its precursors 7-DHC and desmosterol (Figure 7). For more precise and accurate measurements it will be necessary to optimise the chromatography to separate these isomers and to reduce tailing of highly abundant cholesterol. Levels of cholesterol were of the order of 500 – 2,500 ng/mm^2 and of 7-DHC plus desmosterol 2 – 10 ng/mm^2.

Application of MALDI-MS for cholesterol analysis

As an alternative to µLESA-nano-LC-MS for MSI of cholesterol we have explored the possibility of exploiting MALDI-MSI. Using on-tissue EADSA as described above but with minor modifications to sample preparation it was possible to image the $[M]^+$ ion of GP-derivatised cholesterol (Figure 9).

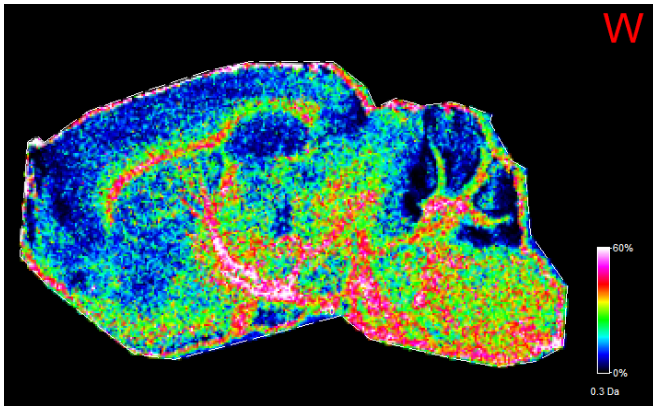

Figure 9. MALDI-MSI of the $[M]^+$ ion cholesterol.

Oxysterols in CYP46A1-/- mouse brain

The high concentration of 24S-HC compared to other oxysterols makes the identification of minor and closely eluting oxysterols difficult. To overcome this problem, we have taken advantage of brain tissue from the *CYP46A1-/-* which is reported to be essentially devoid to 24S-HC [Lund 2003, Meljon 2014, Mast 2017b]. Analysis of the same brain regions as for WT mouse confirmed an absence of 24S-HC in the *CYP46A1-/-* animal but revealed a minor amount of 25-HC (0.04 ng/mm^2) and 24R-HC (0.02 ng/mm^2). Both these oxysterols were detected at low levels in an earlier study of homogenised *CYP46A1-/-* mouse brain [Meljon 2014]. As in the WT mouse minor low levels of 3β,7α-diHCA plus 7αH,3O-CA were found in cerebellum (0.02 ng/mm^2).

Earlier studies have shown that the cholesterol content of whole brain does not differ significantly between WT and *CYP46A1-/-* animals [Lund 2003, Mast 2017] this was explained by a reduction of cholesterol synthesis compensating for reduced metabolism in the CYP46A1-/- animal.

Acknowledgements

This work was supported by the UK Biotechnology and Biological Sciences Research Council (BBSRC, grant numbers BB/I001735/1 and BB/N015932/1 to WJG, BB/L001942/1 to YW). RA holds a Sêr Cymru Fellowship supported by the Welsh Government and the European Regional Development Fund. Work in IP's laboratory is supported by the National Institute of Health (grant number R01 GM062882). Members of the European Network for Oxysterol Research (ENOR, https://www.oxysterols.net/) are thanked for informative discussions.

References

Oxysterols: modulators of cholesterol metabolism and other processes. Schroepfer GJ Jr. Physiol Rev. 2000 Jan;80(1):361-554.
Five decades with oxysterols. Björkhem I. Biochimie. 2013 Mar;95(3):448-54.
Oxysterols: Old Tale, New Twists. Luu W, Sharpe LJ, Capell-Hattam I, Gelissen IC, Brown AJ. Annu Rev Pharmacol Toxicol. 2016;56:447-67.
Crossing the barrier: oxysterols as cholesterol transporters and metabolic modulators in the brain. Björkhem I. J Intern Med. 2006 Dec;260(6):493-508.
Cholesterol 24-hydroxylase: an enzyme of cholesterol turnover in the brain. Russell DW, Halford RW, Ramirez DM, Shah R, Kotti T. Annu Rev Biochem. 2009;78:1017-40.
Activation of the nuclear receptor LXR by oxysterols defines a new hormone response pathway. Lehmann JM, Kliewer SA, Moore LB, Smith-Oliver TA, Oliver BB, Su JL, Sundseth SS, Winegar DA, Blanchard DE, Spencer TA, Willson TM. J Biol Chem. 1997 Feb 7;272(6):3137-40.

Liver X receptors in the central nervous system: from lipid homeostasis to neuronal degeneration. Wang L, Schuster GU, Hultenby K, Zhang Q, Andersson S, Gustafsson JA. Proc Natl Acad Sci U S A. 2002 Oct 15;99(21):13878-83.

Sterol-regulated transport of SREBPs from endoplasmic reticulum to Golgi: oxysterols block transport by binding to Insig. Radhakrishnan A, Ikeda Y, Kwon HJ, Brown MS, Goldstein JL. Proc Natl Acad Sci U S A. 2007 Apr 17;104(16):6511-8.

The effect of 24S-hydroxycholesterol on cholesterol homeostasis in neurons: quantitative changes to the cortical neuron proteome. Wang Y, Muneton S, Sjövall J, Jovanovic JN, Griffiths WJ. J Proteome Res. 2008 Apr;7(4):1606-14.

Changes in the levels of cerebral and extracerebral sterols in the brain of patients with Alzheimer's disease. Heverin M, Bogdanovic N, Lütjohann D, Bayer T, Pikuleva I, Bretillon L, Diczfalusy U, Winblad B, Björkhem I. J Lipid Res. 2004 Jan;45(1):186-93.

Cytochrome P450 27A1 Deficiency and Regional Differences in Brain Sterol Metabolism Cause Preferential Cholestanol Accumulation in the Cerebellum. Mast N, Anderson KW, Lin JB, Li Y, Turko IV, Tatsuoka C, Bjorkhem I, Pikuleva IA. J Biol Chem. 2017a Mar 24;292(12):4913-4924.

Cholestenoic acids regulate motor neuron survival via liver X receptors. Theofilopoulos S, Griffiths WJ, Crick PJ, Yang S, Meljon A, Ogundare M, Kitambi SS, Lockhart A, Tuschl K, Clayton PT, Morris AA, Martinez A, Reddy MA, Martinuzzi A, Bassi MT, Honda A, Mizuochi T, Kimura A, Nittono H, De Michele G, Carbone R, Criscuolo C, Yau JL, Seckl JR, Schüle R, Schöls L, Sailer AW, Kuhle J, Fraidakis MJ, Gustafsson JÅ, Steffensen KR, Björkhem I, Ernfors P, Sjövall J, Arenas E, Wang Y. J Clin Invest. 2014 Nov;124(11):4829-42.

7α-hydroxy-3-oxo-4-cholestenoic acid in cerebrospinal fluid reflects the integrity of the blood-brain barrier. Saeed A, Floris F, Andersson U, Pikuleva I, Lövgren-Sandblom A, Bjerke M, Paucar M, Wallin A, Svenningsson P, Björkhem I. J Lipid Res. 2014 Feb;55(2):313-8.

Novel route for elimination of brain oxysterols across the blood-brain barrier: conversion into 7alpha-hydroxy-3-oxo-4-cholestenoic acid. Meaney S, Heverin M, Panzenboeck U, Ekström L, Axelsson M, Andersson U, Diczfalusy U, Pikuleva I, Wahren J, Sattler W, Björkhem I. J Lipid Res. 2007 Apr;48(4):944-51.

Thematic review series: brain Lipids. Cholesterol metabolism in the central nervous system during early development and in the mature animal. Dietschy JM, Turley SD. J Lipid Res. 2004 Aug;45(8):1375-97.

Sterol metabolism disorders and neurodevelopment-an update. Kanungo S, Soares N, He M, Steiner RD. Dev Disabil Res Rev. 2013;17(3):197-210.

Oxysteroids: a new class of steroids with autocrine and paracrine functions. Javitt NB. Trends Endocrinol Metab. 2004 Oct;15(8):393-7.

Cholesterolomics: An update. Griffiths WJ, Abdel-Khalik J, Yutuc E, Morgan AH, Gilmore I, Hearn T, Wang Y. Anal Biochem. 2017 May 1;524:56-67.

Cell-specific discrimination of desmosterol and desmosterol mimetics confers selective regulation of LXR and SREBP in macrophages. Muse ED, Yu S, Edillor CR, Tao J, Spann NJ, Troutman TD, Seidman JS, Henke A, Roland JT, Ozeki KA, Thompson BM, McDonald JG, Bahadorani J, Tsimikas S, Grossman TR, Tremblay MS, Glass CK. Proc Natl Acad Sci U S A. 2018 Apr 9. pii: 201714518. doi: 10.1073/pnas.1714518115. [Epub ahead of print].

Sterol intermediates from cholesterol biosynthetic pathway as liver X receptor ligands. Yang C, McDonald JG, Patel A, Zhang Y, Umetani M, Xu F, Westover EJ, Covey DF, Mangelsdorf DJ, Cohen JC, Hobbs HH. J Biol Chem. 2006 Sep 22;281(38):27816-26.

Analysis of tissue specimens by matrix-assisted laser desorption/ionization imaging mass spectrometry in biological and clinical research. Norris JL, Caprioli RM. Chem Rev. 2013 Apr 10;113(4):2309-42.

MALDI imaging of lipid biochemistry in tissues by mass spectrometry. Berry KA, Hankin JA, Barkley RM, Spraggins JM, Caprioli RM, Murphy RC. Chem Rev. 2011 Oct 12;111(10):6491-512.
MALDI imaging mass spectrometry: spatial molecular analysis to enable a new age of discovery. Gessel MM, Norris JL, Caprioli RM. J Proteomics. 2014 Jul 31;107:71-82.
Matrix-assisted laser desorption/ionisation mass spectrometry imaging of lipids in rat brain tissue with integrated unsupervised and supervised multivariant statistical analysis. Trim PJ, Atkinson SJ, Princivalle AP, Marshall PS, West A, Clench MR. Rapid Commun Mass Spectrom. 2008 May;22(10):1503-9.
MALDI mass spectrometric imaging of lipids in rat brain injury models. Hankin JA, Farias SE, Barkley RM, Heidenreich K, Frey LC, Hamazaki K, Kim HY, Murphy RC. J Am Soc Mass Spectrom. 2011 Jun;22(6):1014-21.
Spatial organization of lipids in the human retina and optic nerve by MALDI imaging massspectrometry. Zemski Berry KA, Gordon WC, Murphy RC, Bazan NG. J Lipid Res. 2014 Mar;55(3):504-15.
Profiling and Imaging Ion Mobility-Mass Spectrometry Analysis of Cholesterol and 7-Dehydrocholesterol in Cells Via Sputtered Silver MALDI. Xu L, Kliman M, Forsythe JG, Korade Z, Hmelo AB, Porter NA, McLean JA. J Am Soc Mass Spectrom. 2015 Jun;26(6):924-33.
Mass spectrometry imaging of rat brain lipid profile changes over time following traumatic brain injury. Roux A, Muller L, Jackson SN, Post J, Baldwin K, Hoffer B, Balaban CD, Barbacci D, Schultz JA, Gouty S, Cox BM, Woods AS. J Neurosci Methods. 2016 Oct 15;272:19-32.
Laser Desorption/Ionization Mass Spectrometric Imaging of Endogenous Lipids from Rat Brain Tissue Implanted with Silver Nanoparticles. Muller L, Baldwin K, Barbacci DC, Jackson SN, Roux A, Balaban CD, Brinson BE, McCully MI, Lewis EK, Schultz JA, Woods AS. J Am Soc Mass Spectrom. 2017 Aug;28(8):1716-1728.
Mass spectrometry imaging for dissecting steroid intracrinology within target tissues. Cobice DF, Mackay CL, Goodwin RJ, McBride A, Langridge-Smith PR, Webster SP, Walker BR, Andrew R. Anal Chem. 2013 Dec 3;85(23):11576-84
Spatial Localization and Quantitation of Androgens in Mouse Testis by Mass Spectrometry Imaging. Cobice DF, Livingstone DE, Mackay CL, Goodwin RJ, Smith LB, Walker BR, Andrew R. Anal Chem. 2016 Nov 1;88(21):10362-10367
Quantification of 11β-hydroxysteroid dehydrogenase 1 kinetics and pharmacodynamic effects of inhibitors in brain using mass spectrometry imaging and stable-isotope tracers in mice. Cobice DF, Livingstone DEW, McBride A, MacKay CL, Walker BR, Webster SP, Andrew R. Biochem Pharmacol. 2018 Feb;148:88-99.
The use of hydrazine-based derivatization reagents for improved sensitivity and detection of carbonyl containing compounds using MALDI-MSI. Flinders B, Morrell J, Marshall PS, Ranshaw LE, Clench MR. Anal Bioanal Chem. 2015 Mar;407(8):2085-94.
Derivatization Strategies for the Detection of Triamcinolone Acetonide in Cartilage by Using Matrix-Assisted Laser Desorption/Ionization Mass Spectrometry Imaging. Barré FP, Flinders B, Garcia JP, Jansen I, Huizing LR, Porta T, Creemers LB, Heeren RM, Cillero-Pastor B. Anal Chem. 2016 Dec 20;88(24):12051-12059.
Microscopic visualization of testosterone in mouse testis by use of imaging mass spectrometry. Shimma S, Kumada HO, Taniguchi H, Konno A, Yao I, Furuta K, Matsuda T, Ito S. Anal Bioanal Chem. 2016 Nov;408(27):7607-7615. Epub 2016 May 26. Erratum in: Anal Bioanal Chem. 2016 Nov;408(27):7881.
Reactions of microsolvated organic compounds at ambient surfaces: droplet velocity, charge state, and solvent effects. Badu-Tawiah AK, Campbell DI, Cooks RG. J Am Soc Mass Spectrom. 2012 Jun;23(6):1077-84.

Liquid microjunction surface sampling probe electrospray mass spectrometry for detection of drugs and metabolites in thin tissue sections. Van Berkel GJ, Kertesz V, Koeplinger KA, Vavrek M, Kong AN. J Mass Spectrom. 2008 Apr;43(4):500-8.

Quantitative spatial analysis of the mouse brain lipidome by pressurized liquid extraction surface analysis. Almeida R, Berzina Z, Arnspang EC, Baumgart J, Vogt J, Nitsch R, Ejsing CS. Anal Chem. 2015 Feb 3;87(3):1749-56.

Liquid chromatography-mass spectrometry utilizing multi-stage fragmentation for the identification of oxysterols. Karu K, Hornshaw M, Woffendin G, Bodin K, Hamberg M, Alvelius G, Sjövall J, Turton J, Wang Y, Griffiths WJ. J Lipid Res. 2007 Apr;48(4):976-87.

Highly automated nano-LC/MS-based approach for thousand cell-scale quantification of side chain-hydroxylated oxysterols. Roberg-Larsen H, Lund K, Vehus T, Solberg N, Vesterdal C, Misaghian D, Olsen PA, Krauss S, Wilson SR, Lundanes E. J Lipid Res. 2014 Jul;55(7):1531-6.

Quantitative charge-tags for sterol and oxysterol analysis. Crick PJ, William Bentley T, Abdel-Khalik J, Matthews I, Clayton PT, Morris AA, Bigger BW, Zerbinati C, Tritapepe L, Iuliano L, Wang Y, Griffiths WJ. Clin Chem. 2015 Feb;61(2):400-11.

Evaluation of novel derivatisation reagents for the analysis of oxysterols. Crick PJ, Aponte J, Bentley TW, Matthews I, Wang Y, Griffiths WJ. Biochem Biophys Res Commun. 2014 Apr 11;446(3):756-61.

Transcriptional and post-translational changes in the brain of mice deficient in cholesterol removal mediated by cytochrome P450 46A1 (CYP46A1). Mast N, Lin JB, Anderson KW, Bjorkhem I, Pikuleva IA. PLoS One. 2017b Oct 26;12(10):e0187168.

Integration of Ion Mobility MS_E after Fully Automated, Online, High-Resolution Liquid Extraction Surface Analysis Micro-Liquid Chromatography. Lamont L, Baumert M, Ogrinc Potočnik N, Allen M, Vreeken R, Heeren RMA, Porta T. Anal Chem. 2017 Oct 17;89(20):11143-11150.

Protein identification in imaging mass spectrometry through spatially targeted liquid micro-extractions. Ryan DJ, Nei D, Prentice BM, Rose KL, Caprioli RM, Spraggins JM. Rapid Commun Mass Spectrom. 2018 Mar 15;32(5):442-450.

Cerebrospinal fluid steroidomics: are bioactive bile acids present in brain? Ogundare M, Theofilopoulos S, Lockhart A, Hall LJ, Arenas E, Sjövall J, Brenton AG, Wang Y, Griffiths WJ. J Biol Chem. 2010 Feb 12;285(7):4666-79

Oxysterols in the brain of the cholesterol 24-hydroxylase knockout mouse. Meljon A, Wang Y, Griffiths WJ. Biochem Biophys Res Commun. 2014 Apr 11;446(3):768-74.

Cholesterol metabolites exported from human brain. Iuliano L, Crick PJ, Zerbinati C, Tritapepe L, Abdel-Khalik J, Poirot M, Wang Y, Griffiths WJ. Steroids. 2015 Jul;99(Pt B):189-93.

Knockout of the cholesterol 24-hydroxylase gene in mice reveals a brain-specific mechanism of cholesterol turnover. Lund EG, Xie C, Kotti T, Turley SD, Dietschy JM, Russell DW. J Biol Chem. 2003 Jun 20;278(25):22980-8.